EVOLUTIONARY CHARACTERISTICS OF RIPPLES GENERATED BY DISTURBANCE WAVES IN ANNULAR FLOW

S.V. ALEKSEENKO[1,2], A.V. CHERDANTSEV[1,2,c], O.M. HEINZ[1], S.M. KHARLAMOV[1,2], D.M. MARKOVICH[1,2]

[1]Kutateladze Institute of Thermophysics, Novosibirsk, 630090, Russia
[2]Novosibirsk State University, Novosibirsk, 630090, Russia

[c]Corresponding author: Tel.: +73833325678; Fax: +73833356684; Email: cherdantsev@itp.nsc.ru

KEYWORDS:
Main subjects: multiphase flow
Fluid: annular gas-liquid flow
Visualization method: laser-induced fluorescence
Other keywords: disturbance waves, ripples, entrainment, image processing

INTRODUCTION: Annular flow is the flow of liquid film along channel walls and high-velocity gas stream in the central part of the channel. At high enough gas and liquid flow rates annular-dispersed flow takes place, characterized by entrainment of liquid from film surface into the core of gas stream. Entrainment is always accompanied by presence of disturbance waves with very high values of amplitude and velocity. Besides disturbance waves, small-scale ripple waves exist at the base film between disturbance waves and at the surface of disturbance waves. One of the entrainment mechanisms is scattering of ripples, travelling over the disturbance waves, by intensive gas shear [1].

Entrainment of liquid from liquid film surface in annular gas-liquid flow exerts essential influence on the integral characteristics of flow. Disturbance waves were intensively studied for the last fifty years. It was found that disturbance waves travel with nearly constant velocity over long (several meters) distances. Various data on the average amplitude, velocity, frequency and spacing of disturbance waves in various conditions are available in literature [2-6]. Ripples were studied in relatively small number of works [e.g., 7], independently on disturbance waves. Normally, measurements techniques with low spatial resolution (mostly, conductance probes of various types) were used. In the signal of such probes disturbance waves look like single-humped solitary waves with steep front and flat rear slope, and the ripples, covering disturbance waves, are nearly absent. Such representation is used in models of entrainment, where only the disturbance waves are taken into account, and the ripples are neglected [e.g., 8, 9]. Works with high spatial resolution [10-11] show that the disturbance waves are covered by fast ripples, and the amplitude of these ripples is comparable to that of disturbance waves.

Recently, experimental system for field measurements of liquid film thickness was developed based on laser-induced fluorescence technique [12]. Analysis of both spatial and temporal evolution of film surface showed that the ripples are generated at the back slopes of the disturbance waves. Subsequently, the ripples can either travel over the base film between the disturbance waves and be absorbed by the next disturbance wave (‘slow ripples’), or travel over disturbance waves and disappear near its front (‘fast ripples’). Disappearance of the fast ripples was related to scattering of the fast ripples by the gas shear into droplets.

In present work, new automatic algorithm, based on cross-correlation analysis and statistical treatment, is developed for studying the ripples, generated by the disturbance waves, taking into account their evolution.

EXPERIMENTAL SETUP AND MEASUREMENT TECHNIQUE: Experiments were conducted in downward annular flow in vertical Plexiglas pipe with inner diameter d=15 mm. Liquid was introduced as a film through ring-slot distributor, so that the annular flow regime took place from the liquid inlet. Area of measurements was located 50-60 cm below the inlet. Water and two water-glycerol solutions with kinematic viscosity ν=1.5 and $1.9*10^{-6}$ m^2/s – were used as working liquids. Range of superficial gas velocities was 27-58 m/s, range of liquid film Reynolds numbers ($Re=q/\pi d\nu$, where q – volumetric liquid flow rate) was 142-350.

Laser-induced fluorescence technique was used. Vertical laser sheet enlightened one longitudinal section of the pipe, in order to excite the fluorescence of rhodamin-6G, dissolved in liquid. Local brightness of the fluorescent light was measured by high-speed camera. The brightness was then recalculated into local film thickness, using

calibration curve. Each frame represents instantaneous distribution of local film thickness over the length of 12 cm, measured in 600 points (thus, spatial resolution was 0.2 mm/pixel). Camera frame rate was 10 kHz, exposure varied from 30 to 70 μs. Two 2-second realizations were obtained for each regime point. Details on the measurement technique are given in [12-13].

DATA PROCESSING AND RESULTS: Figure 1 shows an example of evolution of film thickness in both space and time. Horizontal axis corresponds to longitudinal coordinate (total length is 120 mm); vertical axis corresponds to time (total length 52 ms). Brightness is directly proportional to local film thickness. Disturbance wave is seen as wide bright band, moving along the diagonal. It is covered by the fast ripples (short bright bands), which normally appear at the back slope of disturbance wave, moves faster than the disturbance wave and disappears near the front of disturbance wave. The base film is covered by the slow ripples, originating at the back slopes of disturbance waves. Slow ripples decelerate, lagging behind the disturbance waves; then they move with constant speed and are finally absorbed by the following disturbance wave. Narrow bright tracks with very high velocity (large slop to t-axis) represent tracks of entrained droplets.

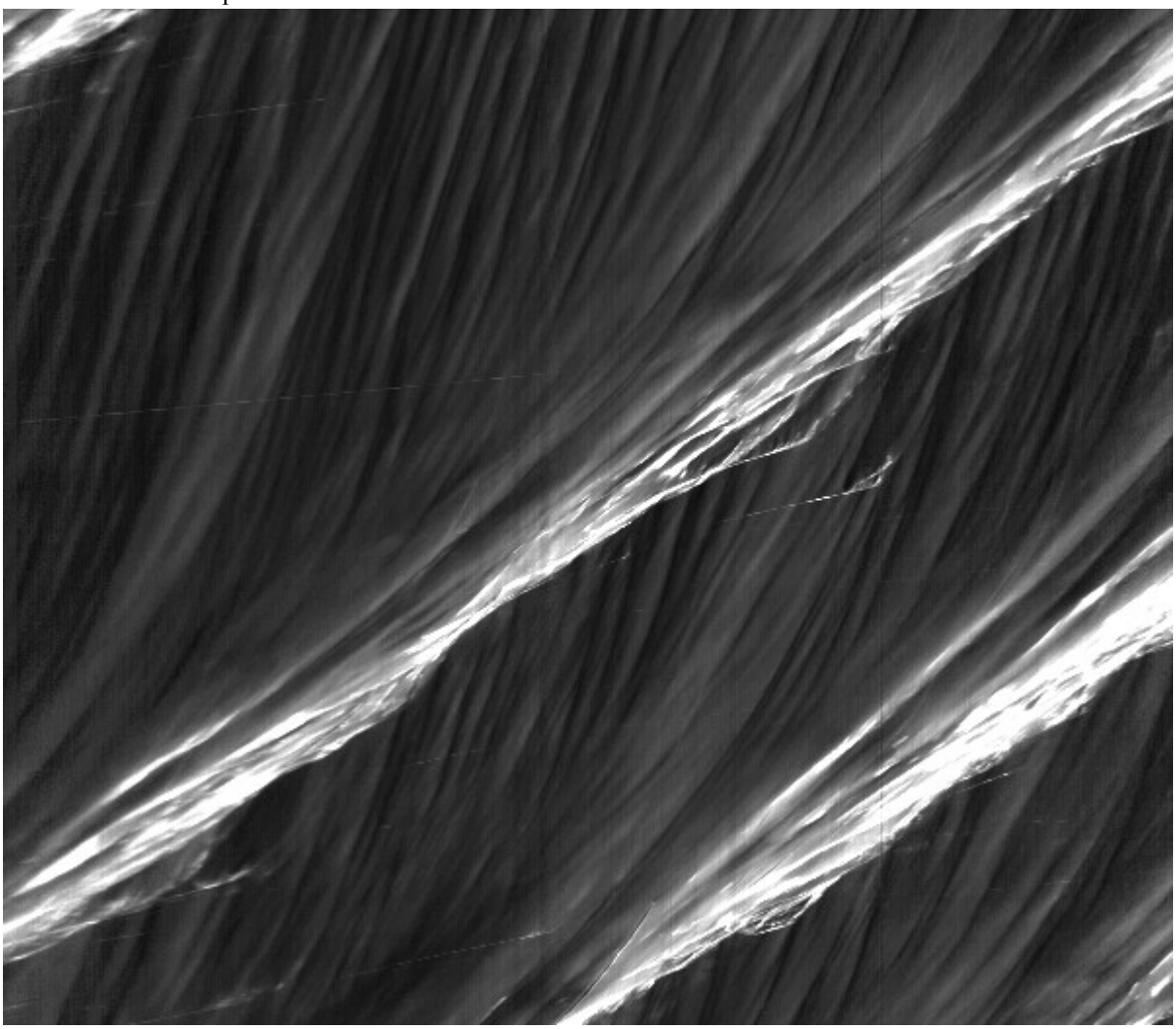

Fig. 1 Example of evolution of film thickness in both space and time. Water, Re=220, Vg=27 m/s.

Automatic search for disturbance waves in $H(t,x)$ surface was based on $H_V(t)$ – the film thickness, averaged over the spatio-temporal trajectory with constant velocity V. This means that for each moment of time t linear trajectory was constructed, which began in the point $\{t,1\}$ and ended in the point $\{t+599/V,600\}$. $H_V(t)$ was the average film thickness in the 600 points, belonging to the trajectory. Cross-correlation velocity was used as V, since it is expected to be good estimation of the average velocity of disturbance waves. This velocity was obtained by cross-correlating the 'temporal records' (columns of $H(t,x)$). Not less than 20 pairs of such records with different position and separation

distance were processed for each regime point in order to enhance the reliability. It was assumed that disturbance waves belong to the areas where $H_V(t)$ is larger than certain threshold. Threshold value H_{V0} was defined after variation of this value over the whole available range. The value, corresponding to the local minimum of number of waves, was chosen. This value roughly corresponds to the double thickness of the base film, defined as the most probable value of film thickness over the whole matrix $H(t,x)$. This fact agrees to the observations of work [10] that the average thickness of disturbance waves is twice larger than the base film.

The obtained areas (which have shape of parallelogram) with disturbance waves were transformed into rectangles by nullifying the temporal shift with changing x (Figure 2). Since velocities of individual disturbance waves are essentially different from each other, additional correction was needed. For each column of the new rectangular matrix, time moment of maximum film thickness t_{max} was defined. Then the array $t_{max}(x)$ was approximated by the linear fit, which gave for each disturbance wave more precise values of velocity and initial time moment of appearance. For further processing some disturbance waves were filtered out, using sum of the squared errors of linear approximation of $t_{max}(x)$ as a criterion. The most part of such cases was related to the coalescence of disturbance waves. Processing of coalescing waves will be performed in near future.

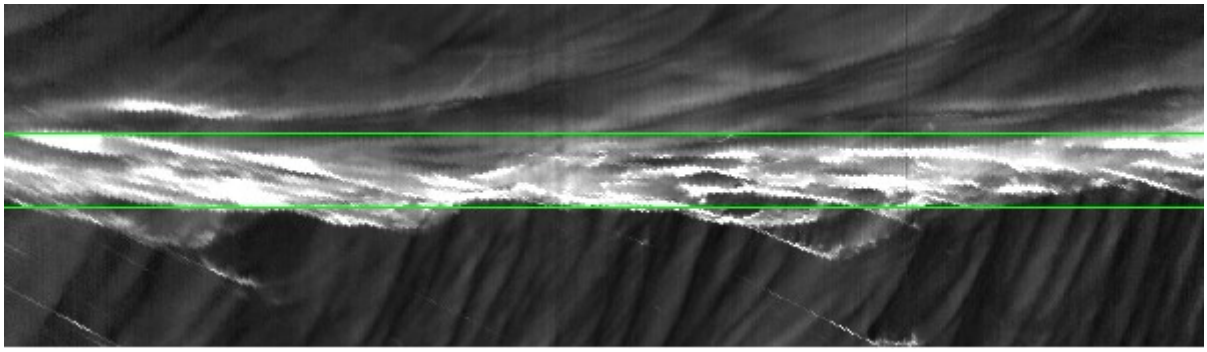

Fig. 2 Disturbance wave from Fig. 1 after transform. Green lines border part of the disturbance wave, covered by fast ripples.

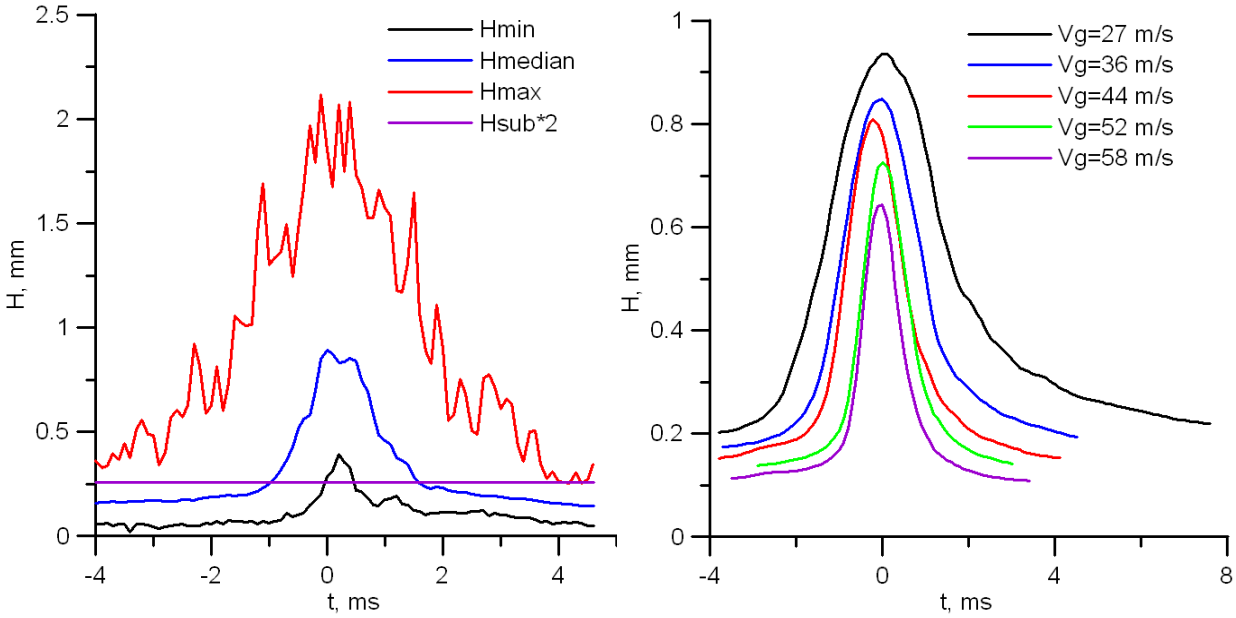

Fig. 3 Left: time profiles of a disturbance wave (minimum, median and maximum thickness at each moment of relative time). The double thickness of substrate is also shown. Water, Re=350, Vg=44 m/s. Right: median time-profiles, averaged by all the disturbance waves for given regime point. Water, Re=350. Waves travel RTL for both cases.

Figure 3 (left) shows three different time-profiles of an individual disturbance wave: maximum, minimum and median value of film thickness at fixed moment of 'relative' time. Points, where the median time-profile crosses the value of the threshold, give good estimate of the part of disturbance wave, covered by the fast ripples (this part is limited by the

green lines in Figure 2). Figure 3 (right) shows the examples of the averaged shape of the median time-profile at different gas velocities.

The matrix *H(t,x)*, constructed for the slow ripples processing, begins right after the end of the previous disturbance wave (Figure 4). For each moment of time, three values were determined: 1) mean film thickness 2) standard deviation of film thickness, which could serve as the rough estimation of the amplitude of the slow ripples 3) velocity of ripples. The latter was defined by cross-correlating two rows of the new matrix *H(t,x)*, separated by 10 rows (1 ms). Velocity of slow ripples in laboratory system is defined as $V_r=V_r'*V_d/(V_r'+V_d)$, where V_d is velocity of the disturbance wave, and V_r' is velocity of slow ripples in transformed system.

Fig. 4 Part of the base film right after the disturbance wave from figures 1 and 2, transformed in the same manner. Water, Re=220, Vg=27 m/s.

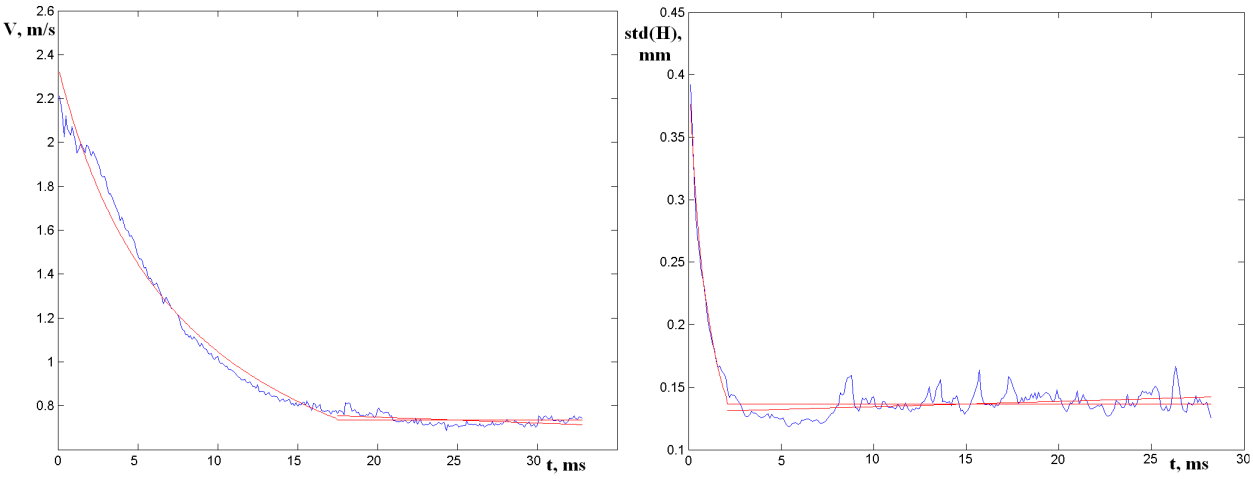

Fig. 5 Left: Evolution of velocity of slow ripples (left) and standard deviation of film thickness (right) with time lag behind the disturbance wave. Left: Water, Re=220, Vg=27 m/s. Right: WGS, $\nu=1.9*10^{-6}$ m^2/s, Re=142, Vg=36 m/s.

Finally, the dependences of each parameter on relative *t* are averaged over the whole number of matrices of the base film. Thus, evolution of the three parameters with time from the disturbance wave can be investigated.

Figure 5 shows the dependence of velocity and amplitude of slow ripples on time from the disturbance wave. It can be seen that two stages can be distinguished: the 'decay' stage and the 'stationary' stage. The two stages can be

approximated by hyperbolic profile and by a constant, respectively. To point of transition was identified based on the criterion of minimum sum of squared deviations of both approximations.

Thus, three zones can be identified in the wavy structure of liquid film: 'body' of disturbance wave, which is covered by the fast ripples; 'tail' of disturbance wave, where slow ripples appear and suffer essential changes of their initial properties; the base film, where velocity and amplitude of slow ripples do not suffer substantial changes. Average time-length of the first part is marked by squares in the Figure 6. Total length of disturbance waves ('body'+'tail') using three different ways of 'tail' definition (by average film thickness, amplitude and velocity of slow ripples) is given in the same figure. Velocity of slow ripples requires the largest time length to reach stationary value; this length is about 3-4 times greater than time-length of the 'body' of disturbance wave. Mean film thickness and ripples amplitude reach stationary values faster; this time-length is nearly the same as the time-length of the 'body'.

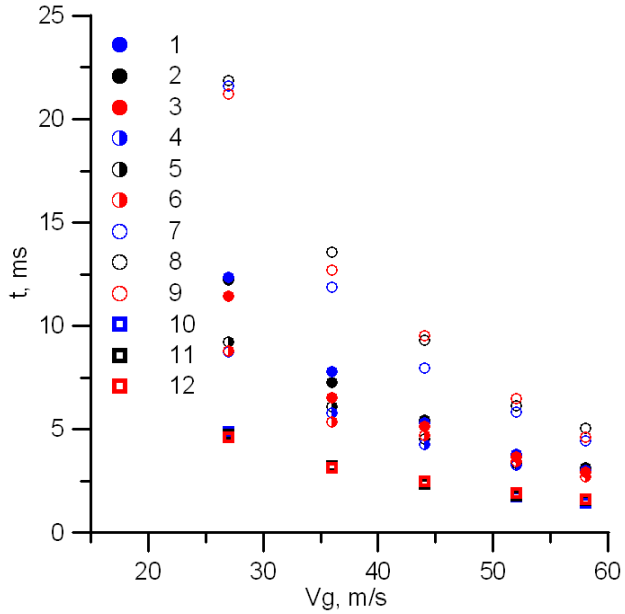

Fig. 6 Time-length of disturbance waves and their tails, data for water. 1,4,7,10 – Re=142; 2,5,8,11 – Re=220; 3,6,9,12 – Re=350. 1-3 – Time-length of velocity stabilization + 'body'; 4-6 – Time-length of mean film thickness stabilization + 'body'; 7-9 – Time-length of film thickness deviation stabilization + 'body'; 10-12 – time-length of the 'body' – highest part of disturbance waves.

Figure 7 (left) shows data on velocity of disturbance waves, initial and final velocity of slow ripples. All the quantities linearly grow with gas velocity and only slightly depend on liquid flow rate. Figure 7 (right) shows height of disturbance waves (defined as maximum height of generalized portrait of disturbance wave, see Fig. 3 (right)); film thickness at the transition from body to tail of disturbance wave; thickness of base film. It is interesting that all the quantities are described by the linear dependence on gas velocity.

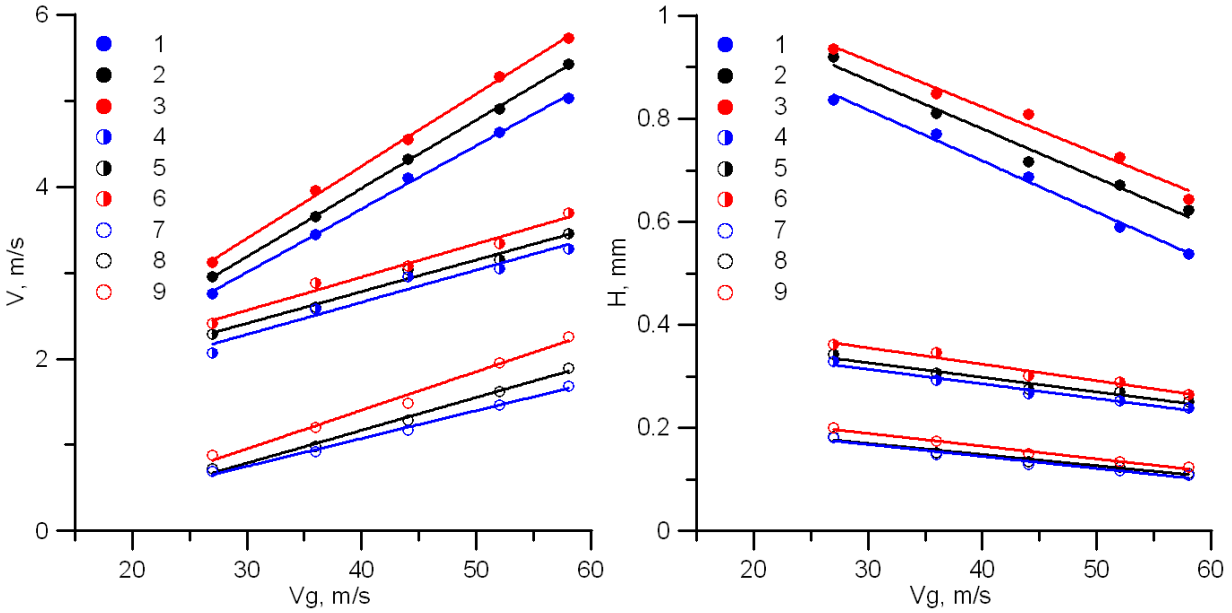

Fig. 7 Properties of waves at the 'stationary' base film. Water. 1,4,7 – Re=142; 2,5,8 – Re=220; 3,6,9 – Re=350. Left: 1-3 – average velocity of disturbance waves. 4-6 – initial velocity of slow ripples; 7-9 – stationary velocity of slow ripples. Right: 1-3 – average height of disturbance waves; 4-6 – film thickness at the edge of disturbance wave; 7-9 – stationary thickness of the base film.

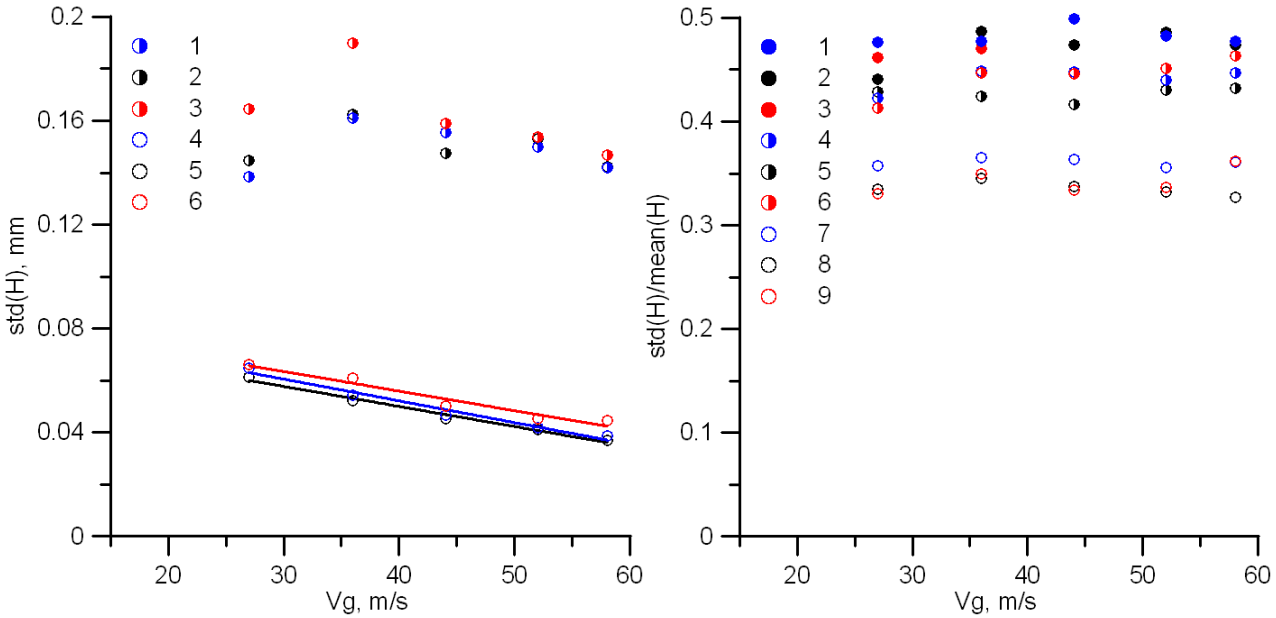

Fig. 8 Amplitude of waves at the 'stationary' base film. 1,4,7 – Re=142; 2,5,8 – Re=220; 3,6,9 – Re=350. Left: Water. 1-3 – film thickness deviation at the edge of disturbance wave; 4-6 – film thickness deviation at the base film. Right: Film thickness deviation at the base film, related to the mean thickness of the base film. 1-3 – water, 4-6 – WGS, $\nu=1.5*10^{-6}$ m^2/s, 7-9 – WGS, $\nu=1.9*10^{-6}$ m^2/s.

Figure 8 shows the stationary amplitude of slow ripples in comparison to the initial amplitude of slow ripples (left) and the relation of the stationary amplitude of slow ripples to the mean thickness of the base film. This ratio (roughness of film surface) doesn't depend on gas velocity and liquid flow rate. This observation qualitatively corresponds to the observations made in [10], but quantitatively the ratio in our experiments is slightly higher (0.35 instead of 0.3 for water, and even higher values for more viscous liquids).

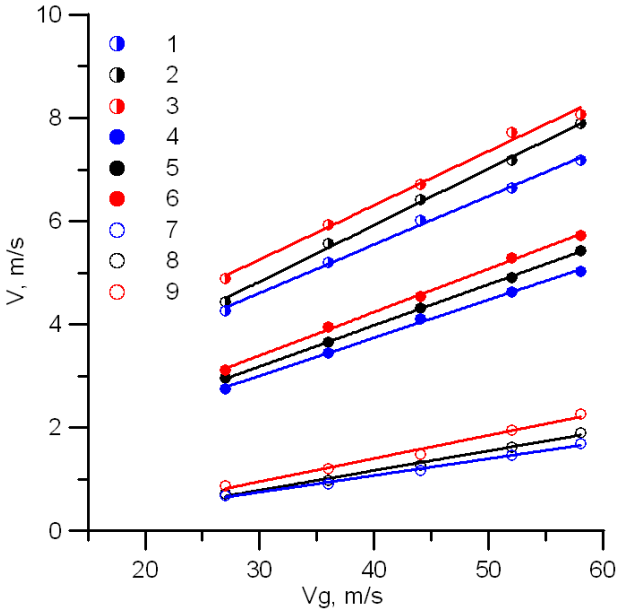

Fig. 9 Velocity of fast ripples (1-3) in comparison to the velocity of disturbance waves (4-6) and slow ripples (7-9). Water. 1,4,7 – Re=142; 2,5,8 – Re=220; 3,6,9 – Re=350.

The velocity of fast ripples was also measured using cross-correlation technique. For all the pairs of time moments, separated by 0.2 ms, velocity was determined using the same formula as that of slow ripples. Then the median value of all the measured velocities, satisfying physical limitation: Vfr>Vd, was used as velocity of fast ripples. Figure 9 shows that this velocity behaves itself similar to the velocity of disturbance waves, overcoming it approximately 1.5 times.

CONCLUSIONS: Field measurements of local film thickness in annular gas-liquid flow were performed, giving possibility to investigate evolution of waves of different types in both space and time. New algorithm of data processing is developed, based on spatio-temporal behavior of waves; in particular, film thickness, averaged over characteristic line, was used as a criterion of waves identification. Three zones were identified: 'body' of disturbance wave, covered by the fast ripples; 'tail' of disturbance wave, where slow ripples are generated and where their properties suffer substantial changes; and the base film, where these properties are nearly stationary. Length of stabilization of velocity of slow ripples was found to be the largest in comparison to the other parameters of slow ripples. Relative interfacial roughness of the base film was found to be independent on gas and liquid flow rates, but to be increasing with liquid viscosity. Velocity of fast ripples was also measured.

Automatic search for the disturbance waves in process of coalescence and investigation of frequency characteristics of fast and slow ripples are related to the future work, as well as the amplitude characteristics of fast ripples that will require to involve additional considerations.

ACKNOWLEDGEMENTS: The work was supported by RF President (grants MK-115.2011.8 and NSh-6686.2012.8) and Russian Foundation for Basic Research (grant 10-08-01145a).

References

1. Woodmansee, D.E., Hanratty, T.J. *Mechanism for the removal of droplets from a liquid surface by a parallel air flow.* Chem Engng Sci, 1969, **24**, p. 299-307.
2. Azzopardi, B.J. *Drops in annular two-phase flow.* Int. J. Mult. Flow 1997, **23 Suppl**, p. 1-53
3. Han, H. et al.. *A study on the effect of gas flow rate on the wave characteristics in two-phase gas–liquid annular flow.* Nucl. Engng. Des. 2006, **236**, p. 2580–2588
4. Sawant, P. et al.. *Properties of disturbance waves in vertical annular two-phase flow*. Nucl. Engng. Des. 2008, **238,** p. 3528–3541.
5. Belt, R.J. et al. *Time and spatially resolved measurements of interfacial waves in vertical annular flow*. Int. J. Mult. Flow 2010, **36**, p. 570–587

6. Al-Sarkhi, A. et al. *Inclination effect on waves characteristics in annular two-phase flow.* AIChE J. 2012, **58,** p. 1018-1029.
7. Chu, K.J., Dukler, A.E. *Statistical characteristics of thin, wavy liquid film. II. Studies of substrate and its wave structure*. AIChE J. 1974, **20**, p. 695-706.
8. Baniamerian, Z., Aghanajafi, C. *Studying the influence of refrigerant type on thermal efficiency of annular two-phase flows; mass transfer viewpoint.* Korean J. Chem. Eng. 2011, **28**, p. 49-55
9. Ryu, S.-H., Park, G.-C. *A droplet entrainment model based on the force balance of an interfacial wave in two-phase annular flow.* Nucl. Eng. Des. 2011, **241**, p. 3890-3897
10. Schubring, D. et al. *Planar laser-induced fluorescence (PLIF) measurements of liquid film thickness in annular flow. Part I: methods and data.* Int. J. Mult. Flow 2010, **36**, p. 815-824.
11. Farias, P. S. C. et al. *Liquid film characterization in horizontal, annular, two-phase, gas–liquid flow using time-resolved laser-induced fluorescence*. Exp. Fluids 2012, 52 (3), p. 633-645
12. Alekseenko, S.V. et al. *Investigation of waves interaction in annular gas-liquid flow using high-speed fluorescent visualization technique.* Microgravity Sci. Technol. 2008, **20**, p. 271-275.
13. Alekseenko, S.V. et al. *Application of a high-speed laser-induced fluorescence technique for studying the three-dimensional structure of annular gas–liquid flow.* Exp. Fluids 2011, DOI: 10.1007/s00348-011-1200-5